Reconfiguration of NASA GRC's Vacuum Facility 6 for Testing of Advanced Electric Propulsion System (AEPS) Hardware

IEPC-2017-028

Presented at the 35th International Electric Propulsion Conference
Georgia Institute of Technology • Atlanta, Georgia • USA
October 8 – 12, 2017

Peter Y. Peterson[1]
Vantage Partners, LLC
NASA Glenn Research Center, Cleveland, OH, 44135

and

Hani Kamhawi[2], Wensheng Huang[3], John Yim[4], Tom Haag[5], Jonathan Mackey[6], Mike McVetta[7], Luke Sorrelle[8], Tom Tomsik[9], Ryan Gillagan[10], and Daniel Herman[11]
NASA Glenn Research Center, Cleveland, OH, 44135

Abstract: The NASA Hall Effect Rocket with Magnetic Shielding (HERMeS) 12.5 kW Hall thruster has been the subject of extensive technology maturation in preparation for development into a flight propulsion system. The HERMeS thruster is being developed and tested at NASA GRC and NASA JPL through support of the Space Technology Mission Directorate (STMD) and is intended to be used as the electric propulsion system on the Power and Propulsion Element (PPE) of the recently announced Deep Space Gateway (DSG). The Advanced Electric Propulsion System (AEPS) contract was awarded to Aerojet-Rocketdyne to develop the HERMeS system into a flight system for use by NASA. To address the hardware test needs of the AEPS project, NASA GRC launched an effort to reconfigure Vacuum Facility 6 (VF-6) for high-power electric propulsion testing including upgrades and reconfigurations necessary to conduct performance, plasma plume, and system level integration testing. Results of the verification and validation testing with HERMeS Technology Demonstration Unit (TDU)-1 and TDU-3 Hall thrusters are also included.

I. Introduction

FOR missions beyond low Earth orbit, spacecraft size and mass can be dominated by onboard chemical propulsion systems and propellants that may constitute more than 50 percent of spacecraft mass. This impact can be substantially reduced through the utilization of Solar Electric Propulsion (SEP) due to its substantially higher specific

[1] Senior Research Engineer, Electric Propulsion Systems Branch, peter.y.peterson@nasa.gov
[2] Senior Research Engineer, Electric Propulsion Systems Branch, hani.kamhawi-1@nasa.gov
[3] Research Engineer, Electric Propulsion Systems Branch, wensheng.huang@nasa.gov
[4] Research Engineer, Electric Propulsion Systems Branch, john.t.yim@nasa.gov
[5] Senior Research Engineer, Electric Propulsion Systems Branch, thomas.w.haag@nasa.gov
[6] Research Engineer, Electric Propulsion Systems Branch, jonathan.a.mackey@nasa.gov
[7] Mechanical Engineer, Experimental Facility Branch, michael.s.mcvetta@nasa.gov
[8] Electrical Engineer, Experimental Facility Branch, luke.t.sorrelle@nasa.gov
[9] Senior Research Engineer, Gas and Fluids System Branch, thomas.m.tomsik@nasa.gov
[10] Research Engineer, Gas and Fluids System Branch, ryan.p.gilligan@nasa.gov
[11] Research Engineer, Electric Propulsion Systems Branch, daniel.a.herman@nasa.gov

impulse. Studies performed for NASA's Human Exploration and Operations Mission Directorate (HEOMD) and Science Mission Directorate have demonstrated that a 40 kW-class SEP capability can be enabling for both near term and future architectures and science missions [1].

Since 2012 NASA has been developing a 14 kW Hall thruster electric propulsion string that can serve as the building block for realizing a 40 kW-class SEP capability. NASA continues to evolve a human exploration approach for beyond low-Earth orbit and to do so, where practical, in a manner involving international, academic, and industry partners [3]. NASA publicly presented a reference exploration concept at the HEOMD Committee of the NASA Advisory Council meeting on March 28, 2017 [4]. This approach is based on an evolutionary human exploration architecture, depicted in Figure 1, expanding into the solar system with cis-lunar flight testing and validation of exploration capabilities before crewed missions beyond the earth-moon system and eventual crewed Mars missions. One of the key objectives is to achieve human exploration of Mars and beyond through the prioritization of those technologies and capabilities best suited for such a mission in accordance with the stepping stone approach to exploration [5]. High-power solar electric propulsion is one of those key technologies that has been prioritized because of its significant exploration benefits. A high-power, 40 kW-class Hall thruster propulsion system provides significant capability and represents, along with flexible blanket solar array technology, a readily scalable technology with a clear path to much higher power systems.

The 14 kW Hall thruster system development, led by the NASA Glenn Research Center and the Jet Propulsion Laboratory, began with maturation of the high-power Hall thruster and power processing unit. The technology development work has transitioned to Aerojet Rocketdyne via a competitive procurement selection for the Advanced Electric Propulsion System (AEPS) contract. The AEPS contract includes the development, qualification, and multiple flight 14 kW electric propulsion string deliveries. The AEPS Electric Propulsion (EP) string consists of the Hall thruster, power processing unit (including digital control and interface functionality), xenon flow controller, and associated intra-string harnesses. NASA continues to support the AEPS development leveraging in-house expertise, plasma modeling capability, and world-class test facilities. NASA also executes AEPS and mission risk

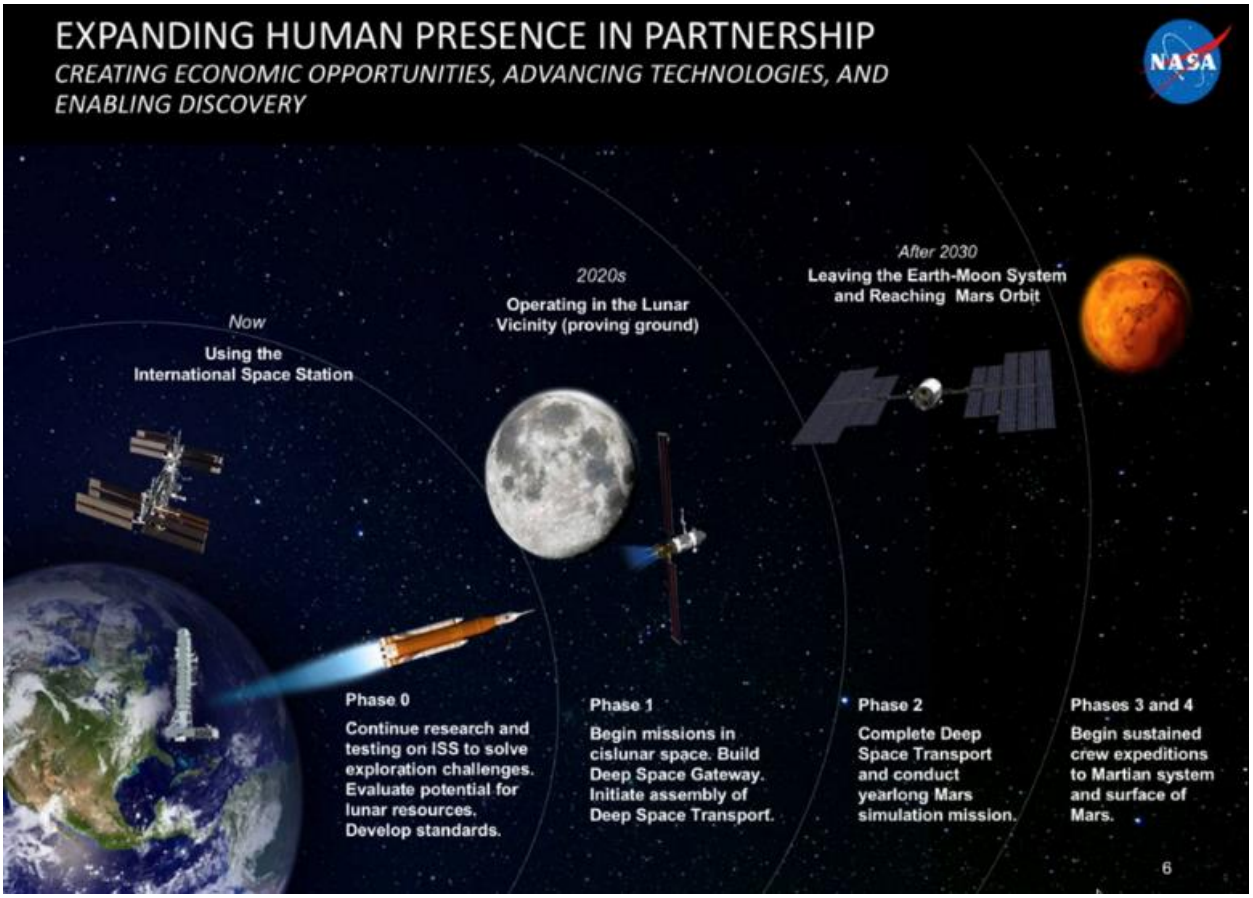

Figure 1. NASA Human Exploration Vision including Deep Space Gateway (DSG) and Deep Space Transport (DST) [2].

reduction activities to support the AEPS development and mission application. It was determined that reconfiguring GRC's Vacuum Facility 6 (VF-6) to accommodate high-power Hall thruster performance, plasma plume, and system level integration testing could provide an additional schedule and cost risk reductions to the project. This paper details the reconfiguration made to VF-6 and provides results of the verification and validation testing with HERMeS Technology Demonstration Unit (TDU) -1 and TDU-3 Hall thrusters.

II. NASA GRC Vacuum Facility 6

NASA GRC VF–6 is a 7.6 m diameter by 21 m long thermal vacuum facility located at NASA GRC (Figure 2). VF-6 capabilities include a Liquid Nitrogen (LN2) cooled shroud capable providing 240 kW of thermal rejection and spans the entire length of the vacuum chamber. It also includes a solar simulator that can provide concentrated power equivalent to Earth and Mercury orbit solar input with a one degree subtense angle. VF-6 is evacuated from atmosphere to a rough vacuum by four 87 kL/min Roots blowers backed by three 24 kL/min mechanical pumps. High-vacuum is achieved by twelve cryopumps that reach a no-gas load base pressure is 3.7×10^{-7} Torr-air which correspond to a pumping speed of approximately 900,000 L/s on air and approximately 380,000 L/s on xenon (prior to VF-6 reconfiguration).

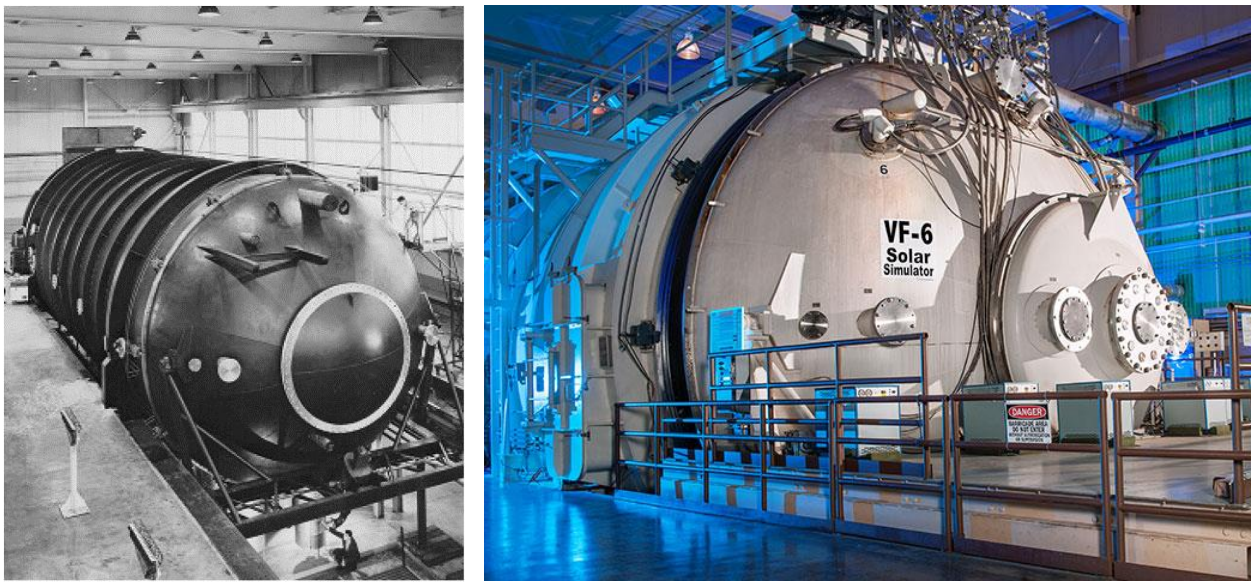

Figure 2, NASA Vacuum Facility 6 during construction circa 1961 (left) [6] and a recent photograph (right).

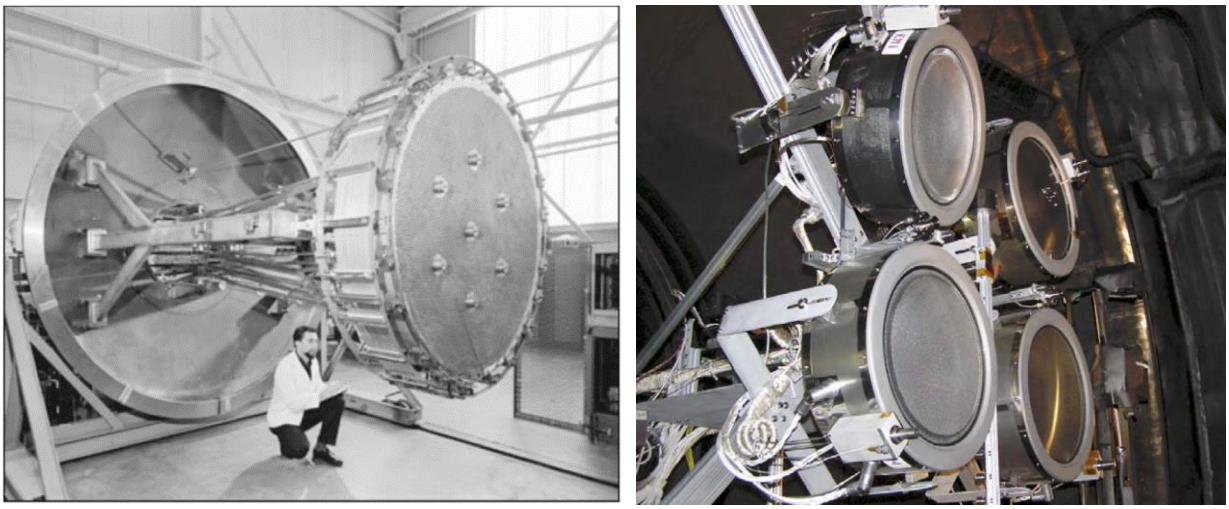

Figure 3. 1.5-m diameter mercury ion thruster (circa 1968) and a NEXT multi-thruster array testing (circa 2006) in VF-6.

NASA VF-6 has a long history of providing high-vacuum environmental testing capabilities for EP activities, thermal vacuum, in-space simulation of solar radiance, power conversion testbed, and solar power conversion by both solar arrays and solar thermal. Of note, VF-6 was a key facility used to conduct a variety of tests to evaluate prototype solar array modules, thermal shielding materials, communication devices, and a variety of other sensors and components for NASA's MESSENGER spacecraft [7]. In 2003, VF-6 was used for the flight antenna qualification and final solar thermal vacuum tests for the MESSENGER spacecraft [8]. VF-6 has also been used for multiple EP development campaigns over the past fifty years including a 200 kW mercury ion thruster in 1968, a multi-thruster array of 7 kW NEXT ion thrusters in 2006 [6] (Figure 3), and a low-power anode layer Hall thruster in 2001 [9].

A. Reconfiguration of VF-6 for high-power Hall thruster testing

The goal of the VF-6 reconfiguration was to bring the additional vacuum facility on-line for high-power Hall thruster testing and provide a second vacuum facility at NASA GRC for HERMeS and AEPS testing. The primary objective was to reproduce the testing capabilities that currently exist in NASA GRC Vacuum Facility 5 (VF-5) as detailed in Refs [10-15]. NASA GRC VF-5 has been the main vacuum facility employed in the HERMeS thruster development and recent life assessment of the TDU-1 and TDU-3 thrusters [15, 16]. To meet this objective, VF-6 needed to be reconfigured with performance and plasma plume diagnostics, backsputter diagnostics, facility pressure diagnostics, power and propellant systems, both slow- and high-speed telemetry acquisition systems, a video surveillance system and improved vacuum chamber shielding from the sputtering of high-energy accelerated ions from the thruster. Additionally, recent lessons learned in regards to thruster electrical interaction with a grounded vacuum chamber as described in Ref. [11] and providing a low-impedance power transmission as described in Ref. [17] were implemented in the VF-6 reconfiguration.

Figure 4. VF-6 during installation of Grafoil® shielding.

B. VF-6 Reconfiguration

VF-6 underwent several configuration changes to meet the requirements of high-power Hall thruster testing. The primary change was shielding the facility internal surfaces with sputter resistant material to protect the facility from high-energy ions in the plume and thus reduce the amount of backsputtered material that reaches the test hardware. One of the requirements imposed on the AEPS contract was the ability to demonstrate life of the propulsion system in a ground test facility with a backsputter rate of less or equal to 2 μm per 1,000 hours at all throttle conditions. Due to the size of VF-6 and given the planned testing activities for AEPS project, the team determined that shielding would be accomplished with Grafoil® covered aluminum sheet, as shown in Figure 4, instead of the high-density carbon panels used if VF-5 [15]. The AEPS activities in VF-6 will center on short-duration thruster wear tests, near-field plasma property measurements with Laser Induced Florence (LIF), spacecraft main power bus integration testing, AEPS propulsion system integration tests, and acceptance and plasma plume mapping of all HERMeS TDUs. The long duration wear testing of HERMeS and AEPS Hall thrusters will occur in VF-5.

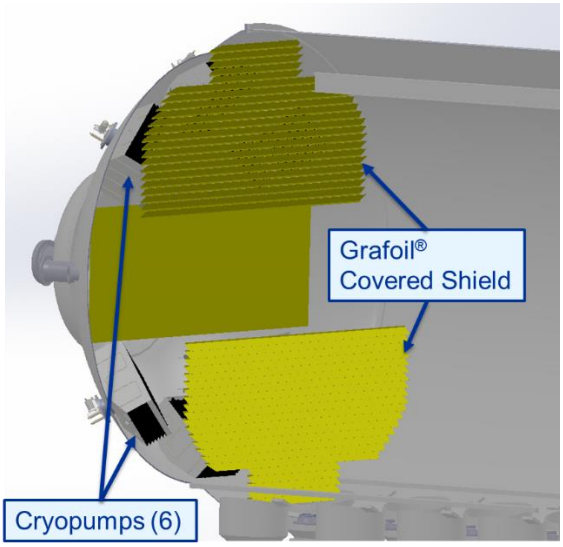

Figure 5. A solid model of VF-6 downstream cryopump shielding.

The second major VF-6 facility reconfiguration change was the installation of plasma plume shielding on eight of the twelve cryopumps. This addressed several concerns of operating high-power EP devices such as thermal loading of the LN2 cryopump shields, minimizing gas conductance loses from pump shielding, and reduction of backsputtered material

from the pump shielding reaching the test hardware. The team employed vacuum facility and back sputtering modeling packages to assess different configurations and find the most appropriate method of shielding the VF-6 cryopumps. The figures of merit used to rank the modeling results included the effective pressure in the vicinity of the test hardware as compared to no shielding, the amount of backsputtered material at the test hardware, and the ease of fabrication of the structure given the mechanical limitation of VF-6 internal mounting fixtures. Several potential shielding designs were considered and the configuration illustrated in Figure 5 for the six downstream cryopumps was selected.

The VF-6 cryopump shielding modeling results indicated that the effective pressure in the vicinity of the test hardware was only increased by approximately 13%, as shown in Figure 6, due to the shielding of the downstream cryopumps. It should be noted that the modeling results in Figure 6 are for shielding of the six downstream cryopumps only and does not include the effect of shielding the two cryopumps located under the Hall thruster. The calculated backsputter rate at the test hardware location was approximately 1.1 μm/khr at the HERMeS thruster maximum power throttle condition of 12.5 kW and discharge voltage of 600 V.

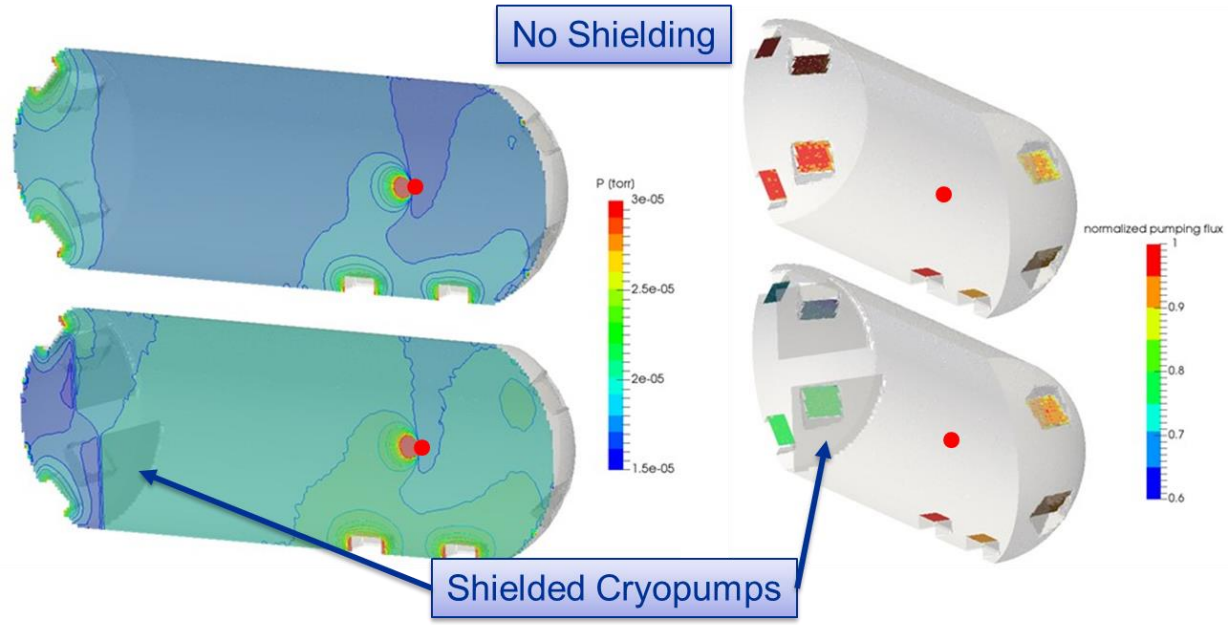

Figure 6. The operating pressure modeling results for VF-6 with (bottom) and without (top) downstream cryopump shields (the red circle represents the Hall thruster).

III. Experimental Apparatus

A. Diagnostics

1. *High-Power Thrust Stand*

The VF-6 thrust stand uses the same inverted pendulum style design as the existing VF-5 high-power thrust stand [18-20], but incorporates several improvements. Figure 8 shows the TDU and thrust stand mounted on an extruded aluminum structural framework. This thrust stand framework was designed to be structurally independent from the plasma plume diagnostic structural framework to reduce vibration noise. The internal sensors and external thermal housing were thermally controlled by a cooling loop. Three stainless-steel electro-polished propellant lines pass through the stand, inside the thermal housing. The power electrical pass-through, commonly referred to as a "waterfall", was located along the side and underneath the thrust stand, which provided improved access to the electrical connections and thrust stand service panels.

Instrumentation of the thrust stand includes the same sensors and actuators as the heritage VF-5 thrust stand with the addition of secondary displacement and inclination sensors and a calibration homing sensor. The secondary displacement sensor installed uses a laser triangulation method to measure the physical distance and transmit digitally to the thrust stand controller. The secondary inclination sensor uses an inertial inclination sensing circuit with an analog output to the controller while the homing sensor uses a photoelectric sensor to provide a homing signal for the calibration string.

During performance mapping activities, the thrust stand was calibrated in-situ with calibrated masses on a pulley system connected to a stepper motor. The thrust stand was calibrated before and after each performance mapping period or at the beginning and end of each day of performance testing depending on the length of the performance testing. The VF-6 thruster stand has shown to be as capable and accurate as the VF-5 thrust stand with a thrust uncertainty <1%. This thrust uncertainty was based on a statistical analysis of the calibration and thrust zero data taken throughout the verification and validation test campaign.

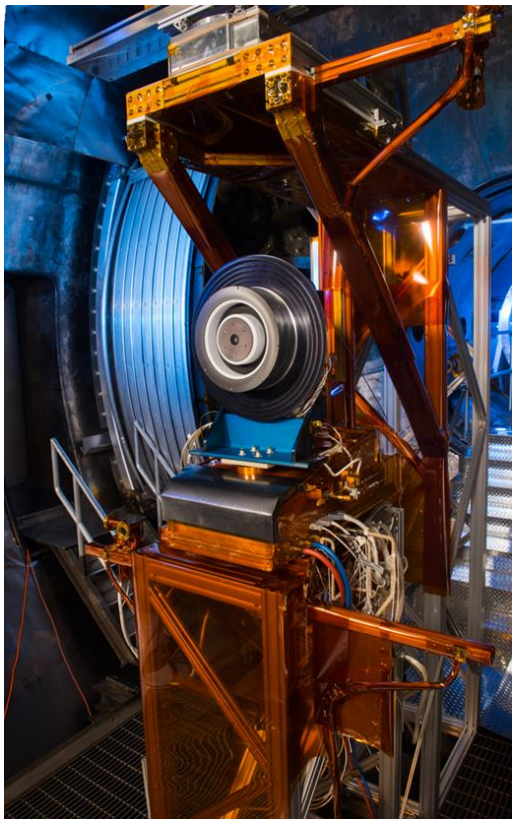

Figure 7. High-power thruster stand installed in VF-6 with the TDU-3 Hall thruster.

2. *Plasma Diagnostics*

This plasma diagnostics system consisted of a set of plasma probes at the end of a probe arm mounted to a linear stage and a rotary stage, which allowed the probes to be swept around the thruster (-122° to 120°, firing axis at 0°) at different distances (750 to 1497 mm). Positioning accuracy of this motion system was <1 mm for the radial axis and <0.2° for the polar axis. The plasma probes include a Faraday Probe (FP), a Langmuir Probe (LP), a Retarding Potential Analyzer (RPA), and a Wien-Filter Spectrometer (WFS).

Figure 8 shows a photograph of the VF-6 probe package and the relative position of the four probes in the package. This probe package is an updated version of the VF-5 probe package, with spatial offset between the probes adjusted to minimize potential shadowing of one probe by another probe. Both the RPA and WFS were protected by independent shutters. The probe package, boom arm, and the bottom of the motion stages were shielded with a combination of Grafoil® and Kapton®. The Grafoil® reduced the amount of backsputtered material on the probe package and the Kapton® prevents collection of net plasma current.

The FP was a GRC design [21, 22] and was used to measure ion current density in the far-field plume. The collector and guard ring were made of molybdenum. The angular resolution of the FP data was ~0.5°. At each operating condition, the FP was azimuthally swept at five different distances corresponding to 4, 5, 6, 7, and 8 mean channel diameters (MCD). An additional sweep at 8 MCD was conducted to ensure that the data was not dependent on the sweep direction. During testing, measurements were made at different bias voltages in increments of 10 V. The results indicated that -30 V bias with respect to facility ground was sufficient to repel incoming electrons for all operating conditions.

The LP was a disk-shaped molybdenum collector connected to a tungsten central conductor. This probe was primarily used to obtain the local plasma potential so that the RPA data can be corrected by this potential. The LP was swept at 3 Hz for 1 second at each location. A commercial megahertz data acquisition device was used to measure the FP current, LP voltage, and LP current signals.

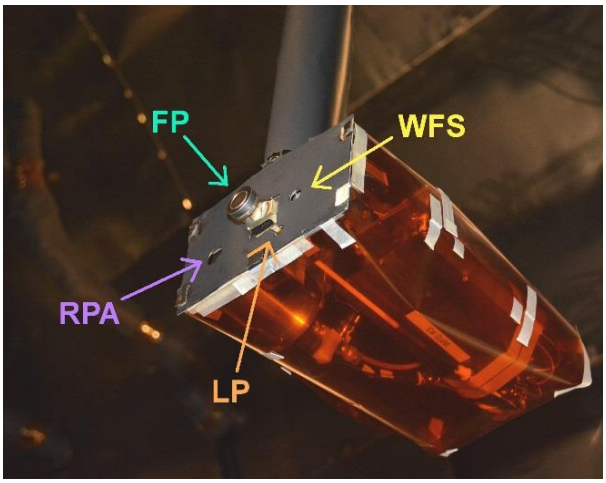

Figure 8. The VF-6 plasma diagnostic probe package.

The RPA was an AFRL design as discussed in Ref.[21, 22]. The RPA was used to measure the ion energy per charge distribution and to identify high energy ions at high angles away from the firing axis. During testing, the electron suppression and repelling grids were biased to -30 V with respect to facility ground, while the ion retarding grid voltage was swept. The ion retarding grid voltage was biased with a sourcemeter while the collected current was measured with a picoammeter. Data were taken at polar angles of ±100°, ±95°, ±90°, ±85°, ±80°, ±75°, ±70°, ±65°, ±60°, ±55°, ±50°, ±45°, ±40°, ±35°, ±30°, ±15°, and 0°.

The WFS was a commercial product and was used to measure charged species current fractions. The WFS was the product from a Small Business Innovation Research contract and has a prior history of usage [21-23]. The electron suppression plate was biased at -30 V with respect to facility ground to suppress secondary electron emission (SEE) from the collector. The main bias plate voltage was swept with a picoammeter, which was also used to measure the collector current. WFS data was collected at 0° for all plasma diagnostic sweeps.

3. *Thruster Surveillance System*

The VF-6 video surveillance system was an upgraded system as compared to the VF-5 system. The cameras were based on a new generation of high definition analog signal technology called Analog High Definition (AHD), which allows a 1080p, 60 Hz signal to be carried over a standard BNC cable. Four AHD cameras were modified for vacuum operation and installed in VF-6 at different locations. The first location was downstream of the thruster on the side wall of VF-6 viewing the test setup. Another camera was mounted in a similar position on the opposite side wall and viewed through an OD2 neutral density filter. A third camera was mounted upstream of the thruster looking at the back of the thruster. A fourth camera was mounted to the corner of the probe arm while viewing the thruster. A set of four video signal splitter/amplifiers were used to route the video signals from the four cameras to two digital video recorders. Each recorder was connected to a high definition monitor. One recorder/monitor set was located in the control room and the other set was located on the outside of VF-6. Figure 9 shows one of the monitors that display the videos from all four cameras simultaneously.

Figure 9. A monitor for the VF-6 surveillance system with a HERMeS TDU under operation.

4. *Time Resolved Thruster Telemetry*

The temporal behavior of the HERMeS Hall thruster key parameters were continuously monitored by multiple oscilloscopes. The oscilloscope telemetry included both AC and DC monitoring of the thruster discharge current and voltage, thruster body voltage and current, cathode-to-ground voltage, and other key cathode parameters. The oscilloscopes internal functionally was used to measure the Root Mean Square (RMS), peak-to-peak (Pk2Pk), and mean value where appropriate. The oscilloscope telemetry was fed into the test data acquisition system and recorded on the same time scale as the rest of the telemetry. The logging of the thruster temporal characteristics provided additional information on the high-speed discharge current-voltage and magnetic field (IVB) sweep that was demonstrated as useful information when interpreting the thruster stability in Refs. [11, 12, 24, 25]. Additionally, a dedicated oscilloscope was used to record high resolution data on the discharge current and voltage for generation of Power Spectrum Density (PSD) plots of the selected operating conditions.

5. *Backsputter Diagnostic*

Three Quartz Crystal Microbalances (QCM) were installed in VF-6 to measure the backsputter flux at the thruster location. All three were positioned approximately 50 mm downstream of the thruster exit plane at a ~1 m radius from the thruster center as shown in Figure 10. All three QCMs were oriented in the downstream direction and were water cooled with three parallel cooling loops from a single chiller. One of the QCMs had a thermocouple to monitor the temperatures to ensure

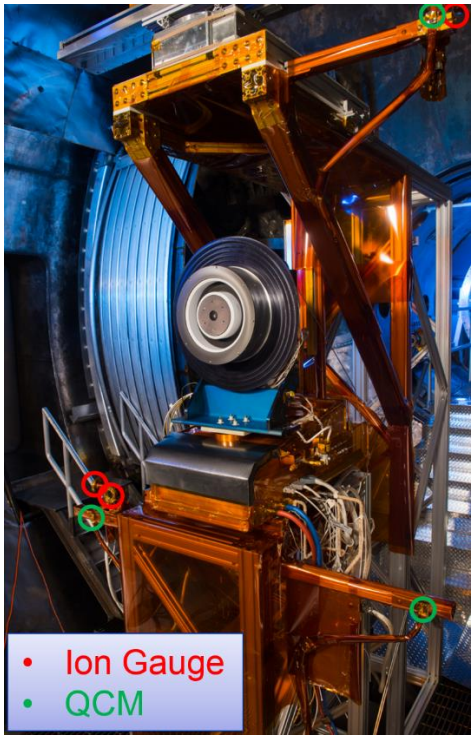

Figure 10. QCM and ion gauge location on the VF-6 test setup.

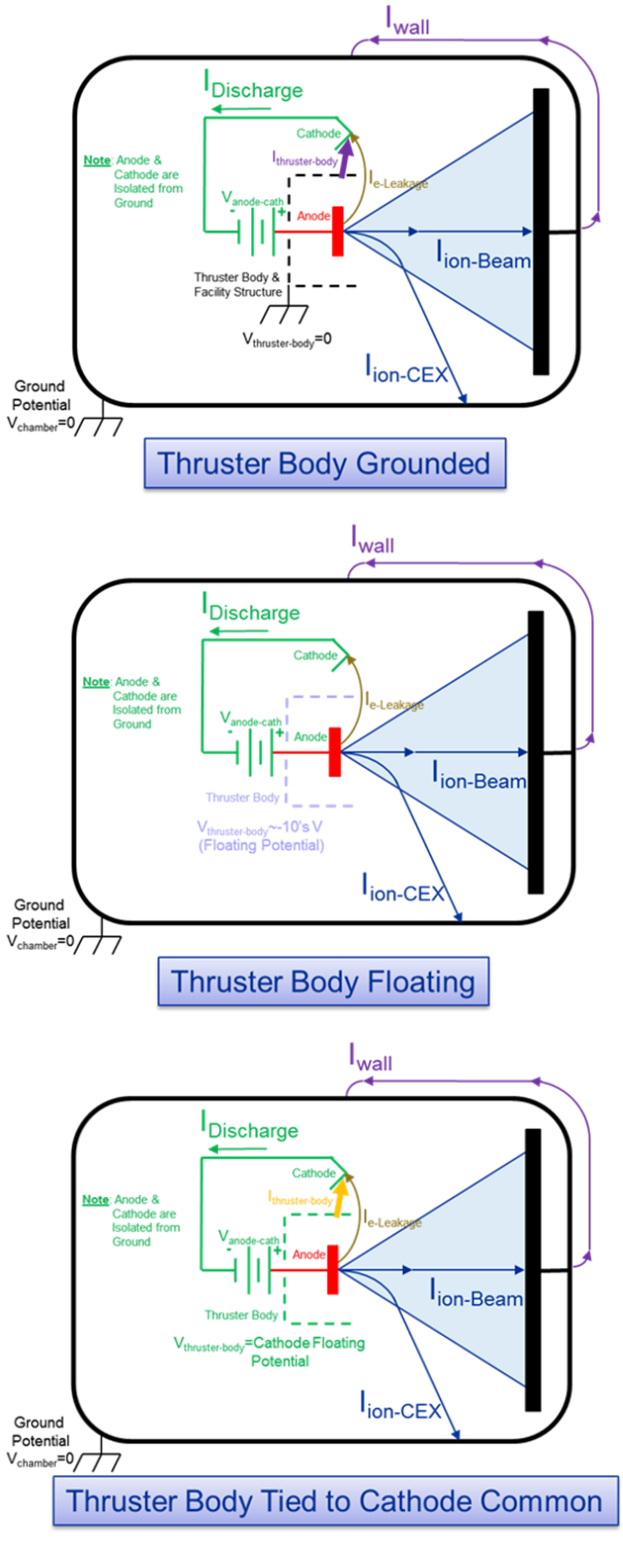

Figure 11. Illustration of a Hall thruster body grounded, body floating, and thruster body tied to cathode common electrical configurations for ground based Hall thruster testing [11].

the cooling loop was operating properly. The QCMs were electrically connected to a digital oscillator unit with a cable restricted to 4 m in length. Since the diameter of VF-6 is too large for the cable to reach a feedthrough panel, the digital oscillator units were placed in the vacuum facility without adverse effects. The QCM controller was interfaced to the main data acquisition system through Ethernet to output the total thickness from all three sensors. The growth rate of thickness can then be post-processed from the raw thickness and time data. The deposition was assumed to be pure carbon.

6. *Pressure Diagnostic*

Three ion gauges were installed in VF-6 to measure the local pressure near the thruster as shown in Figure 11. Two of the gauges were calibrated on nitrogen and located near each other and one of the QCMs. The third ion gauge was calibrated on xenon and located near the other QCM on the top of the thrust stand. Each of the ion gauges were configured for EP operation and had an elbow and plasma screen installed on the inlet of the gauge. A vacuum ISO standard quick release flange adapter was also installed on the opening of each ion gauge to facilitate the in-situ atmospheric testing of each internal ion gauge, to verify operation prior to pump down of the facility. A thermocouple was installed on the exterior of each ion gauge tube and recorded by the main data acquisition system, thus allowing for correlation of the measured pressure during testing. Electrical grounding straps were connected to each internal ion gauge metal housing then to a dedicated facility ground, to ensure that charging effects of the gauges were avoided. The gauge assemblies were then wrapped in dielectric Kapton® to minimize the influence of grounded surfaces on the operation of the Hall thruster. This will be discussed further in the electrical isolation section.

7. *Electrical Configuration*

The electrical configuration of a Hall thruster, in relation to a conducting vacuum facility, has recently been identified as a concern that needs to be considered in the development and qualification of new Hall thruster propulsion systems [11, 25-34]. The electrical configuration of a Hall thruster in a conducting ground based vacuum facility can be described in three configurations (Figure 11);

1. Hall thruster body is electrically tied to the facility ground,
2. Hall thruster body is isolated from the facility ground and allowed to float with respect to the local plasma potential, and
3. Hall thruster body is isolated from the vacuum facility chamber ground and electrically tied to the floating cathode common.

The vast majority of Hall thruster development and qualification testing programs over the past few decades have used the first electrical configuration [35]. In this configuration, it has been demonstrated that the electrons produced by the propulsion system can travel with the ion beam, as well as along alternate low-resistance paths through the conducting thruster body and any nearby grounded structure in close proximity to the thruster. The electrons traveling through the lower resistance path of the chamber walls meet up with the ions in the beam, Charge-Exchange (CEX) ions, on the walls of the chamber, and/or grounded carbon-based beam dump [11, 27, 29, 30, 36].

To reduce the probability of plume electrons traveling through a lower resistance path of the chamber and recombining with the ion beam at the beam dump, and/or chamber walls, the HERMeS and AEPS thrusters have been reconfigured to incorporate the lessons learned in Ref. [11]. The thruster body has been electrically connected to the cathode common and isolated from facility ground. Additionally, all nearby conducting structures and diagnostic equipment were isolated from the thruster plasma plume by a dielectric shield or were floated with respect to ground. This isolation scheme is shown in Figure 7.

8. *Propellant Flow System*

A new laboratory Xenon Flow System (XFS) was built for VF-6 incorporating lessons learned from previous NASA GRC XFS designs and adhering to multiple requirements as described by NASA internal process control documents for hollow cathode operation. The new XFS included design features that enabled switching to a new xenon bottle while maintaining the thruster in an operational state for long duration tests.

The VF-6 XFS employed four xenon mass flow controllers (MFC) including a 50 sccm MFC for the cathode and a 500 sccm MFC for the anode. Additional 500 and 1,000 sccm MFCs were in place to supply xenon to the chamber to elevate pressure during pressure mapping activities. In-situ calibration was accomplished with a NIST traceable mass flow calibration device before and after each testing campaign. The MFC calibration curves indicated that the uncertainty of the anode and cathode flow rates was approximately 1% of the set value.

The gas panel was capable of being baked out, up to 120˚C, via heat tape wrapped around the tubing and valves. The gas panel has terminal connections for gas sampling and a vacuum pump-out fitting with a pressure gauge to read the vacuum pressure in the system during bake-out operations.

9. *Power Supplies, Data Acquisition, and Control System*

A new HERMeS laboratory power console was built for VF-6 including discharge, inner and outer electromagnet, cathode heater, and cathode keeper power supplies. The discharge power supply can output up to 30 kW at 1000 V and 30 A. The console was equipped with a failsafe interlock system that allows the data acquisition system or the VF-6 facility control system to disable power to the thruster in case of a thruster or facility anomaly.

To perform high-speed IVB mapping discussed in Section III.4 above, the HERMeS power console was equipped with a high-speed digital interface connected to the data acquisition control computer. The data acquisition control computer was configured to control the discharge and electromagnet power supplies, such that the IVB sweeps could be automated and monitored by fail-safe limits in the data acquisition system. During IVB data sweep, the control system commanded the magnet power supplies to specified current outputs, then ramped up the discharge voltage over a range at specified increments and dwell times. At each voltage step, the data acquisition control computer recorded a subset of measurements from the data acquisition unit, mass flow control panel, and the oscilloscopes.

The data acquisition system incorporated in the VF-6 reconfiguration was based on the system used on VF-5 high-power Hall thruster test system with improvements based on lessons learned since the start of the HERMeS project. The data acquisition system was based on a commercially available multiplexer system with computer interface. The data acquisition system monitored the voltages, currents, temperatures, propellant flow rates, chamber pressure, and thrust at approximately 1 Hz during performance testing. The computer interface had the additional benefit of allowing a number of channels to be monitored with failsafe limits for unattended operation. The uncertainties of the data acquisition system measurements were ±0.05% for the voltage and current measurements.

A new break-out-box (BOB) was fabricated for the VF-6 reconfiguration effort and is shown in Figure 12. The BOB serves as a single-point location for connecting the power from either a laboratory power console or a Power Processing Unit (PPU) during system integration testing, to the power feed through on the vacuum chamber. The BOB also

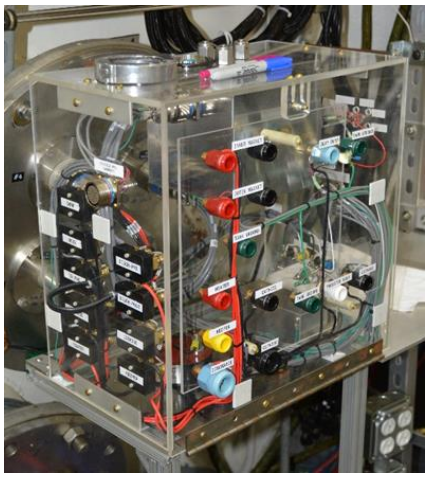

Figure 12. A photograph of VF-6 Break-Out-Box.

serves as a central location of acquiring current and voltage sense line telemetry. The current and voltage sense telemetry was sent to the data acquisition system located adjacent to BOB to reduce the ground-loop noise and to improve noise rejection.

10. *HERMeS Development Hall Thruster*

The test campaign of the reconfigured VF-6 and the new test support hardware, power console, xenon flow system, thrust stand, and plume diagnostics was conducted with the TDU-1 and TDU-3 thrusters. The design of HERMeS incorporates technologies developed by NASA over nearly two decades of research and was enabled by magnetic shielding to effectively eliminate discharge chamber erosion [37-41]. Magnetic shielding significantly increase the operational lifetime compared to state-of-the-art Hall thrusters. HERMeS is capable of operating at 3,000 s specific impulse and its lifetime exceeds 50,000 hours. Initial tests of the HERMeS Hall thruster demonstrated performance, verified magnetic shielding at high specific impulse, and affirmed that the internally mounted cathode minimized the effects of facility pressure on performance. Details regarding TDU thruster design, mission-required operating envelope, and test results were detailed in Refs. [11, 14, 15, 37-39, 42-61]. The HERMeS TDU-3 (Figure 7) includes several new design features compared to TDU-1 that are being assessed to reduction the risk on the AEPS project. These features include flight-like electromagnet coils and a different discharge chamber material (M26 grade Boron Nitride (BN)). Additional details on the HERMeS TDU-3 Hall thruster can be found in Refs. [16, 62, 63].

IV. Results and Discussion

The primary goal this test campaign was to identify any issues with the new setup and to prove that the system was ready for both HERMeS and AEPS testing. This section summarizes TDU-1 and TDU-3 performance, plasma plume, and backsputter results for several Reference Firing Conditions (RFC), detailed in Table 1, and compares them to the results obtained in VF-5.

Table 1. The RFC used during the VF-6 verification and validation testing with both TDU-1 and TDU-3.

Reference Firing Condition (RFC)	Power [kW]	Discharge Voltage [V]
1	1.80	300
2	3.00	300
3	6.25	300
4	8.33	400
5	10.46	500
6	12.50	500
7	12.50	600
8	12.50	700

A. VF-6 Facility Results

The effective pumping speed of VF-6, with the new facility and pump shields, was initially assessed by measuring the background pressure near the test hardware. Through examination of background pressure as a function of xenon mass flow rate, the effective pumping speed was estimated to be 280,000 L/s on xenon. This represents a reduction of approximately 25% compared to previous data collected during NASA's Evolutionary Xenon Thruster (NEXT) testing. While this reduction was greater than the 13% decrease predicted by facility modeling, discussed in Section 0.B, the model only examined the influence of plume shielding the six of the downstream cryopumps. The final configuration of the VF-6 had an additional cryopump shielded from the plasma plume than was originally modeled (Figure 6), which could account for some of the variation of the measured pumping speed compared to the original model. However the effective operating pressure obtained during the test was sufficient for the majority of planned testing in VF-6. Future Hall thruster testing that require vacuum pressures closer to in space conditions (e.g. performance vs. pressure, near field LIF measurements, electrical environment assessment, long duration wear testing, and flight qualification), and/or higher propellant flow rates, will still require the higher pumping speeds of VF-5.

B. Thruster Performance Results

Thruster performance parameters for the HERMeS TDU-1 and TDU-3 thrusters were collected in a series of tests. Figure 13(a) shows the thrust as a function of power measured in VF-6 and compared to data taken in VF-5 with TDU-1 during a 2016 test campaign [12]. The TDU-1 data collected in VF-5 was obtained during performance mapping as a function of the operating pressure. The facility operating pressure at each RFC was independently adjusted by flowing additional xenon into VF-5 to simulate the effect of lower pumping speeds. This method of adjusting operating pressure of a facility has been used by many electric propulsion test campaigns to both baseline the performance as a function of operating pressure and to assess trends from ground based performance to in-space performance [12, 64, 65]. The thrust uncertainty has been found to be approximately ±0.6% for the TDU-1 data in VF-5 and TDU-1 in VF-6. However, the TDU-3 performance data from VF-6 had a larger uncertainty of approximately 5% due to issues with the thrust stand controller and the xenon MFC controller stability, which had been identified and corrected. As mentioned earlier, one of the main goals of this test campaign was to find and correct any issues with the new test setup and support hardware. After corrections were implemented, subsequent testing verified that all issues were successfully addressed. The results presented in Figure 13(a) provide strong evidence that, between the three performances mapping tests in two different vacuum facilities and with two versions of the HERMeS development thrusters, the performance was almost identical and within the uncertainty of the measurements.

Another performance assessment of the TDU-1 and TDU-3 was the ratio of the discharge current to the total mass flow rate (Id/mdot) as a function of the power as shown in Figure 13(b). The Id/mdot provides further insight into the physical processes of testing different Hall thrusters and the dependence on facilities. The trends in Figure 13(b) are in good agreement for most RFCs except for low power conditions. It should be noted that the lower power RFCs also require lower mass flow rates and the variation in the I/mdot could be a result of a non-linear response to background pressure as has been discussed in Refs [64, 66]. Additionally, there was a possibility that the method of increasing facility pressure with xenon injection may be strongly dependent on the configuration of the cryopumping system in each facility, and at the lower flow rate and pressure a deviation I/mdot can be observed.

The relative stability of the thrusters was also examined and the results are presented in Figure 13(c) and (d) by comparing the ratios of the peak-to-peak and RMS discharge current oscillations to discharge current (Id_Pk2Pk/Id

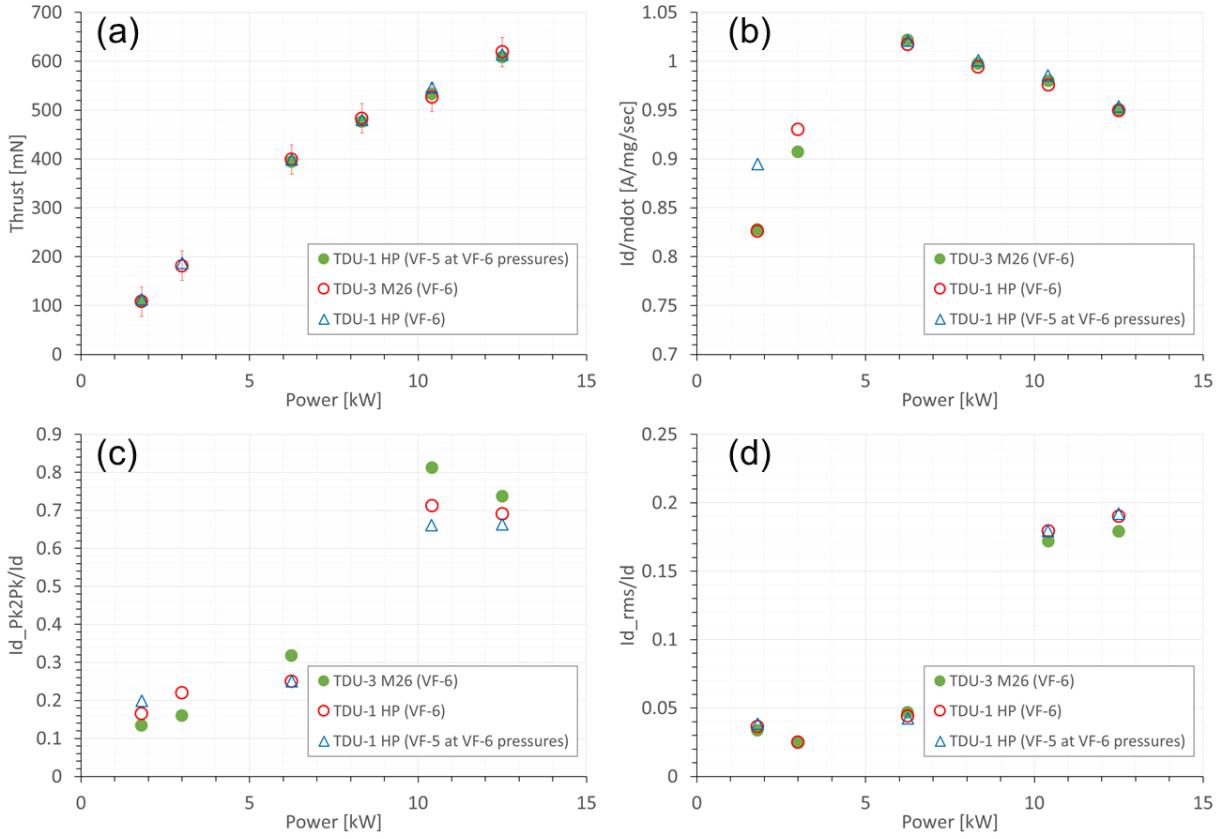

Figure 13. Performance (a, b) and stability results (c, d) of TDU-1 and TDU-3 in VF-6 compared to TDU-1 results from VF-5 at an elevated facility pressure.

and Id_rms/Id). While these two indicators may not provide as much information as a PSD of the discharge current or fast IVB maps, they can still be used as a quick view into the oscillatory nature of the Hall thruster plasma discharge. Examining Figure 13(c) and (d), it was clear that the TDU-1 behaved in a similar manner in VF-6 and VF-5 over the power range of the RFC.

One additionally set of observations can be made in regards to the TDU-1 and TDU-3 performance, I/mdot, and the stability data in Figure 13; and that was changing the grade of BN used in the HERMeS development thruster had a minimal to no impact on the performance of the thruster. While this data was informative, a more detailed testing campaign was conducted in VF-5 comparing the two grades of BN on TDU-3 and results are presented in a companion paper by Kamhawi [63].

C. Plasma Plume Characterization Results

Another objective of the test campaign was to demonstrate that the VF-6 plasma diagnostics functioned consistent with the VF-5 diagnostics system and could properly test the HERMeS thrusters. The plasma diagnostics system served two main purposes in the HERMeS test campaign. The first was to measure the characteristics of the plasma plume from which the state of the thruster can be inferred. The second was to measure the characteristics of energetic ions escaping at high angles from the thruster to support spacecraft interaction and integration studies. To accomplish these, FP and RPA data at high angles was compared for several RFCs.

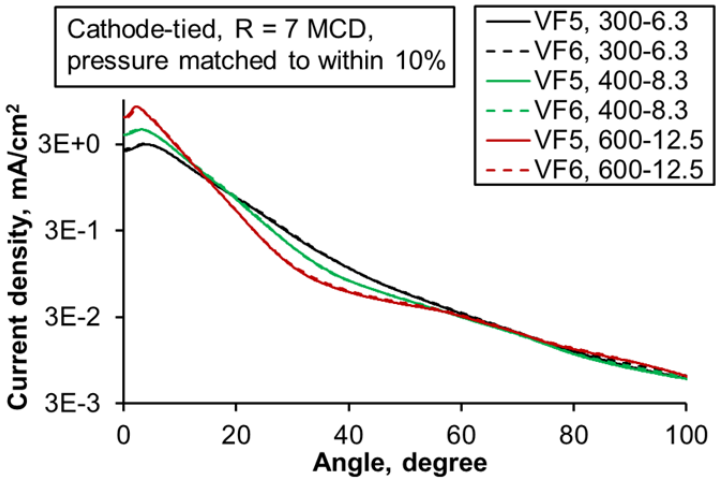

Figure 14. Comparison of current density profiles measured by the VF-5 and VF-6 plasma diagnostics systems.

Figure 14 compares the FP current density measurement between the VF-5 and VF-6 plasma diagnostics systems at a 300 V and 600 V discharge voltage RFCs. The VF-5 data was from the 2016 wear test campaign, detailed in Ref. [11, 12, 15], at an equivalent background pressure to match the VF-6 pumping speed while the VF-6 data was from the current test campaign. The ion current density data matches very closely between the two tests.

Figure 15 compares RPA ion energy per charge spectra between the VF-5 and VF-6 diagnostics system at a 300 V and 600 V discharge voltage RFCs. The farthest off-axis angle on the negative side at which beam energy ions can be detected was used for comparison. This angle was -90° for the 300 V, 6.3 kW RFC and -75° for the 600 V, 12.5 kW RFC. From these two figures, the location and magnitude of the high energy peaks, as well as the shape of the spectra, are in excellent agreement between both diagnostic systems. Data points at approximately 1e-3 energy spectra and below were driven by noise. Nonetheless, it can be concluded that the functionality of the VF6 diagnostics system is consistent with the VF-5 system.

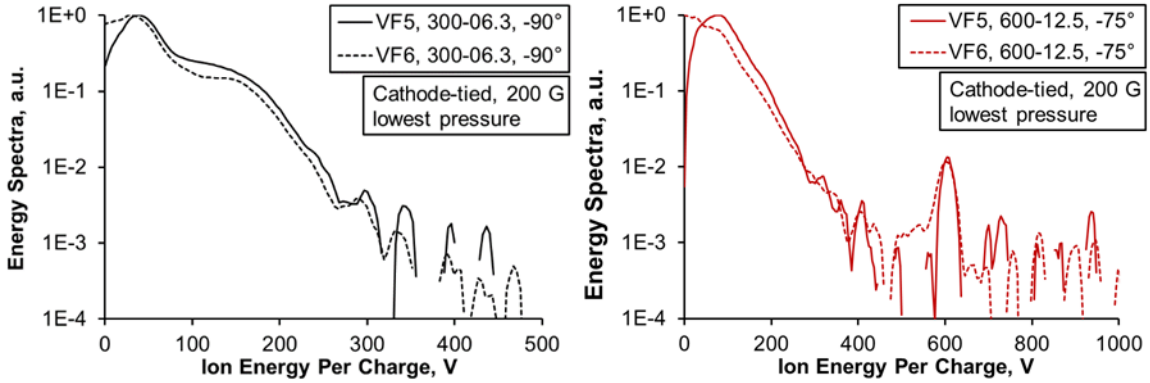

Figure 15. Comparison of ion energy per charge spectra across facilities for the 300 V, 6.3 kW and the 600 V, 12.5 kW RFC.

D. Backsputter Results

A QCM is a precise mass balance that can accurately track the mass added to the sensor over time. To determine a backsputter rate in the vicinity of the test hardware, the composition of the sputtered material was needed to convert the mass data from the QCM into a deposition rate. The theory behind incorporating QCMs as an electric propulsion diagnostic, is described in greater detail in Refs. [67-69]. There are multiple approaches that can be employed to estimate the composition of the backsputter material from post-test analysis of the surface, to knowing the composition of the target material, which, in the case of VF-6 was the recently installed Grafoil® shielding. The backsputter rate of the facility shielding material was monitored and recorded throughout the verification and validation testing in VF-6 with both the TDU-1 and TDU-3 Hall thrusters with three QCM as discussed in Section III.5. Over the course of the VF-6 verification and validation testing, average backsputter rates were determined to be approximately 1.0 μm/khr for the 12.5 kW and 600 V RFC. This result compared very well to the initial modeling backsputter prediction of approximately 1.1 μm/khr.

V. Conclusion

This paper describes NASA GRC efforts to reconfigure VF-6 for high-power Hall thruster testing. Several tests with the HERMeS TDU-1 and TDU-3 Hall thrusters confirmed that the performance and plume data is in good agreement with previous TDU results in VF-5 at equivalent background pressures. The measured effective xenon pumping speed for the reconfigured VF-6 was found to be approximately 280,000 L/s or approximately 25% lower than past data without pump shielding. The measured back sputtering rate near the location of the test hardware was found to be approximately 1.0 μm/khr which matched model results. The addition of VF-6 as a fully capable high-power electric propulsion facility will provide NASA and the AEPS contractor with an additional test facility in which to conduct testing of the AEPS hardware. Two capable facilities at NASA GRC enables parallel development, qualification, and flight acceptance testing to occur in a timely cost-effective manner.

VI. Acknowledgments

The authors would like to thank the Space Technology Mission Directorate in support of the Solar Electric Propulsion Technology Demonstration Mission Project for funding the joint NASA GRC and JPL development of the Advanced Electric Propulsion System. The authors would like to thank Todd Tofil for managing the electric propulsion work within the SEP Project. The authors would also like to thank the many NASA/Aerojet review board members and subject matter experts for providing their expertise and technical guidance to the development of AEPS and its broader Ion Propulsion Subsystem mission application. The authors would like to give a special thank you to Derrick Patterson, Josh Gibson, Dave Yendriga, John Lauerhahs, Natasha Jackson, James Schneider, Larry Hambley, Mike Perez, Matt Daugherty, Jim Szelagowski, Roland Gregg, Terry Jensen, Andrew Sturdivant, Andrew, Mark Forrester, and Elliot Mays for the fabrication, assembly of the test setup, and operation of the vacuum facility.

References

1. Smith, B. K., Nazario, M. L., and Cunningham, C. C. "Solar Electric Propulsion Vehicle Demonstration to Support Future Space Exploration Missions," *Space Propulsion 2012*. Bordeaux, France, 2012.
2. Free, J. "Architecture Status," *NASA Advisory Council Human Exploration and Operations Committee Meeting*. Washington, DC, 2017.
3. Congress, t. "National Aeronautics and Space Administration Transition Authorizatin Act of 2017." 2017.
4. Leiter, H., Kukies, R., Killinger, R., Bonelli, E., Scaranzin, S., Scortecci, F., Neumann, H., and Tartz, M. "RIT-22 Ion Propulsion System: 5,000h Endurance Test Results and Life Prediction." Cincinnati, OH, 2007.
5. Gerstenmaier, W. "Progress in Defining the Deep Space Gateway and Transport Plan," *NASA Advisory Council Human Exploration and Operations Committee Meeting*, 2017.
6. Patterson, M. J., and Sovey, J. S. "History of Electric Propulsion at NASA Glenn Research Center: 1956 to Present," *Journal of Aerospace Engineering* Vol. 26, No. 2, 2013, pp. 300-316.
7. Ercol, C. J., Jenkins, J. E., Dakermanji, G., Santo, A. G., and Mason, L. S. "Prototype Solar Panel Development and Testing for a Mercury Orbiter Spacecraft," *35th Intersociety Energy Conversion Engineering Conference and Exhibit*. Las Vegas, NV, 2000.
8. Keith, S. A. "NASA Glenn Engineers Help Mercury's MESSENGER Prepare For Close Encounter with the Sun." NASA, 2004.

9. Jacobson, D. T., Jankovsky, R. S., Rawlin, V. K., and Manzella, D. H. "High Voltage TAL Performance," *Joint Propulsion Conference, AIAA-01-3777*. AIAA, Salt Lake City, UT, 2001.
10. "NASA GRC Vacuum Facility 5." 2016.
11. Peterson, P. Y., Kamhawi, H., Huang, W., Williams, G., Gilland, J., Yim, J., Hofer, R. R., and Herman, D. "NASA's HERMeS Hall Thruster Electrical Configuration Characterization," *52nd AIAA/ASME/SAE/ASEE Joint Propulsion Conference*. AIAA, Salt Lake City, UT, 2016.
12. Kamhawi, H., Haag, T. W., Huang, W., Herman, D. A., Williams, G. J., Peterson, P. Y., Hofer, R. R., and Mikellides, I. "Performance, Stability, and Pressure Effects Characterization Tests of NASA's 12.5-kW Hall Effect Rocket with Magnetic Shielding (HERMeS) Thruster," *52nd AIAA/SAE/ASEE Joint Propulsion Conference*. Salt Lake City, UT, 2016.
13. Huang, W., Kamhawi, H., and Haag, T. W. "Plasma Oscillation Characterization of NASA's HERMeS Hall Thruster via High Speed Imaging," *52nd AIAA/SAE/ASEE Joint Propulsion Conference*. Salt Lake City, UT, 2016.
14. Kamhawi, H., Haag, T. W., Huang, W., Herman, D. A., Thomas, R., Shastry, R., Yim, J., Chang, L., Clayman, L., Verhey, T. R., Griffiths, C., Myers, J., Williams, G. J., and Mikellides, I. "Performance Characterization of the Solar Electric Propulsion Technology Demonstration Mission 12.5-kW Hall Thruster," *30th International Electric Propulsion Conference*. Kobe, Hyogo, Japan, 2015.
15. Williams, G. J., Gilland, J. H., Peterson, P. Y., Kamhawi, H., Huang, W., Swiatek, M., Joppeck, C., Yim, J., and Haag, T. W. "Wear Testing of the HERMeS Thruster," *52nd AIAA/SAE/ASEE Joint Propulsion Conference*. Salt Lake City, UT, 2016.
16. Williams, G., Gilland, J. H., Kamhawi, H., Choi, M., Peterson, P. Y., and Herman, D. A. "Wear Trends of the HERMeS Thruster as a Function of Throttle Point," *35th International Electric Propulsion Conference*. ERPS, Atlanta, GA, 2017.
17. Pinero, L. "The Impact of Harness Impedance on Hall Thruster Discharge Oscillations," *35th International Electric Propulsion Conference*. ERPS, Atlanta, GA, 2017.
18. Haag, T. W. "Thrust stand for high-power electric propulsion devices," *Review of Scientific Instruments* Vol. 62, No. 5, 1991.
19. Haag, T. W., and Osborn, M. "RHETT/EPDM performance characterization," *International Electric Propulsion Conference, IEPC-97-107*. IEPC-97-102 ed., Cleveland, OH, 1997.
20. Xu, K. G., and Walker, M. L. R. "High-power, null-type, inverted pendulum thrust stand," *Review of Scientific Instruments* Vol. 80, No. 5, 2009.
21. Huang, W., Shastry, R., Soulas, G. C., and Kamhawi, H. "Farfield Plume Measurement and Analysis on the NASA-300M and NASA-300MS," *33rd International Electric Propulsion Conference*. ERPS, Washington, DC, 2013.
22. Huang, W., Kamhawi, H., and Haag, T. "Effect of Background Pressure on the Performance and Plume of the HiVHAc Hall Thruster," *33rd International Electric Propulsion Conference*. ERPS, Washington, DC, 2013.
23. Brown, D. L. "Investigation of Flow Discharge Voltage Hall Thruster Characteristics and Evaluation of Loss Mechanisms," *Aerospace Engineering*. Vol. Doctor of Philosophy, University of Michigan, Ann Arbor, MI, 2009, p. 378.
24. Brown, D. L., and Lobbia, R. B. "Characterization of Hall Thruster Mode Transitions and Facility Interactions," *Joint Army Navy NASA Air Force (JANNAF) conference*. Nashville, TN, 2015.
25. Brown, D. L., Lobbia, R. B., Hartley, K. D., Sekerak, M., King, D., and Peterson, P. Y. "The XR-5 and XR-5A Hall Thrusters, Part 1: Stability and Mode Transitions," *Joint Army Navy NASA Air Force (JANNAF) conference*. Nashville, TN, 2015.
26. Frieman, J. D., King, S. T., Walker, M., Khayms, V., and King, D. "Role of a Conducting Vacuum Chamber in the Hall Effect Thruster Electrical Circuit," *Journal of Propulsion and Power* Vol. 30, No. 6, 2014.
doi: 10.2514/1.B35308
27. Walker, J. A., Frieman, J. D., Walker, M., and Khayms, V. "Hall Effect Thruster Electrical Interaction with a Conductive Vacuum Chamber," *50th AIAA/ASME/SAE/ASEE Joint Propulsion Conference and Exhibit, AIAA-2014-3711*. Cleveland, OH, USA, 2014.
28. Frieman, J. D., King, S. T., Walker, M., Khayms, V., and King, D. "Preliminary Assessment of the Role of a Conducting Vacuum Chamber in the Hall Effect Thruster Electrical Circuit," *50th AIAA/ASME/SAE/ASEE Joint Propulsion Conference and Exhibit, AIAA-2014-3712*. Cleveland, OH, USA, 2014.
29. Walker, J. A., Frieman, J. D., Walker, M., Khayms, V., King, D., and Peterson, P. Y. "Electrical Facility Effects on Hall-Effect-Thruster Cathode Coupling: Discharge Oscillations and Facility Coupling," *Journal of Propulsion and Power*, 2016.
doi: 10.2514/1.B35835
30. Frieman, J. D., Walker, J. A., Walker, M., Khayms, V., and King, D. "Electrical Facility Effects on Hall Thruster Cathode Coupling: Performance and Plume Properties," *Journal of Propulsion and Power* Vol. 32, No. 1, 2016.
doi: 10.2514/1.B35683
31. Sekerak, M., Brown, D. L., Lobbia, R. B., Hartley, K. D., King, D., Peterson, P. Y., Dale, E., Cusson, S., and Gallimore, A. D. "The XR-5 and XR-5A Hall Thrusters, Part 2: Oscillation Behavior," *Joint Army Navy NASA Air Force (JANNAF) conference*. Nashville, TN, 2015.

32. Lobbia, R. B., Brown, D. L., Sekerak, M., Hartley, K. D., King, D., Peterson, P. Y., Dale, E., Cusson, S., and Gallimore, A. D. " The XR-5 and XR-5A Hall Thrusters, Part 3: Time-Resolved Plasma Measurements," *Joint Army Navy NASA Air Force (JANNAF) conference*. Nashville, TN, 2015.
33. Hartley, K. D., Lobbia, R. B., Brown, D. L., Beal, B. E., King, D., Peterson, P. Y., Dale, E., Cusson, S., and Gallimore, A. D. " The XR-5 & XR-5A Hall Thrusters, Part 4: Plume Properties," *Joint Army Navy NASA Air Force (JANNAF) conference*. Nashville, TN, 2015.
34. Katz, I., Lopez Ortega, A., Goebel, D., Sekerak, M., Hofer, R., and Jorns, B. "Performance and Facility Background Pressure Characterization Tests of NASA's 12.5-kW Hall Effect Rocket with Magnetic Shielding Thruster," *14th Spacecraft Charging Technology Conference, ESA/ESTEC,*. Noordwijk, NL USA, 2016.
35. Hofer, R., and Anderson, J. R. "Finite Pressure Effects in Magnetically Shielded Hall Thrusters," *50th AIAA/ASME/SAE/ASEE Joint Propulsion Conference and Exhibit, AIAA-2014-3709*. Cleveland, OH, USA, 2014.
36. McDonald, M. S. "Electron Transport in Hall Thrusters," *Department of Aerospace Engineering*. Vol. Doctorate of Philosophy, The University of Michigan, Ann Arbor, MI, 2012.
37. Hofer, R. R., Kamhawi, H., Mikellides, I., Herman, D. A., Polk, J. E., Huang, W., Yim, J., and Myers, J. "Design Methodology and Scaling of the 12.5 kW HERMeS Hall Thruster for the Solar Electric Propulsion Technology Demonstration Mission," *Presented at the 62nd JANNAF Propulsion Meeting*. Nashville, TN, 2015.
38. Kamhawi, H., Huang, W., Haag, T. W., Yim, J., Chang, L., Clayman, L., Herman, D. A., Shastry, R., Thomas, R., Griffith, C., Myers, J., Williams, G. J., Mikellides, I., Hofer, R. R., Polk, J. E., and Goebel, D. M. "Overview of the Development of the Solar Electric Propulsion Technology Demonstration Mission 12.5-kW Hall Thruster," *50th AIAA/ASME/SAE/ASEE Joint Propulsion Conference*. Cleveland, OH, 2014.
39. Mikellides, I., Hofer, R. R., Katz, I., and Goebel, D. M. "Magnetic Shielding of Hall Thrusters at High Discharge Voltages," *Journal of Applied Physics* Vol. 116, No. 5, 053302, 2013.
40. Kamhawi, H., Manzella, D. H., Smith, T. B., and Schmidt, G. R. "High-Power Hall Propulsion Development at NASA Glenn Research Center," *Space Propulsion 2012*. Bordeaux, France, 2012.
41. Mikellides, I., Katz, I., Hofer, R., Goebel, D., de Grys, K., and Mathers, A. "Magnetic Shielding of the Acceleration Channel Walls in a Long-Life Hall Thruster," *Joint Propulsion Conference, AIAA-10-6942*. Nashville, Tennessee, 2010.
42. Myers, J., Kamhawi, H., and Yim, J. "HERMeS Thermal Model," *51st AIAA/SAE/ASEE Joint Propulsion Conference*. Orlando, FL, 2015.
43. Lopez Ortega, A., Mikellides, I., and Katz, I. "Hall2de Numerical Simulations for the Assessment of Pole Erosion in a Magnetically-Shielded Hall Thruster," *30th International Electric Propulsion Conference*. Kobe, Hyogo, Japan, 2015.
44. Kamhawi, H., Haag, T. W., Huang, W., and Hofer, R. R. "The Voltage-Current Characteristics of the 12.5 kW Hall Effect Rocket with Magnetic Shielding at Different Background Pressure Conditions," *Presented at the 62nd JANNAF Propulsion Meeting*. Nashville, TN, 2015.
45. Hofer, R. R., Kamhawi, H., Herman, D. A., Polk, J. E., Snyder, J. S., Mikellides, I., Huang, W., Myers, J., Yim, J., Williams, G. J., Lopez Ortega, A., Jorns, B., Sekerak, M., Griffiths, C., Shastry, R., Haag, T. W., Verhey, T. R., Gilliam, B., Katz, I., Goebel, D. M., Anderson, J. R., Gilland, J. H., and Clayman, L. "Development Approach and Status of the 12.5 kW HERMeS Hall Thruster for the Solar Electric Propulsion Technology Demonstration Mission," *30th International Electric Propulsion Conference*. Kobe, Hyogo, Japan, 2015.
46. Kamhawi, H., Haag, T., Huang, W., and Hofer, R. R. "The Voltage-Current Characteristics of the 12.5 kW Hall Effect Rocket with Magnetic Shielding at Different Background Pressure Conditions," *62nd JANNAF Propulsion Meeting*. Nashville, TN, 2015.
47. Kamhawi, H., Haag, T., Huang, W., Herman, D. A., Thomas, R., Shastry, R., Yim, J., Chang, L., Clayman, L., Verhey, T., Griffiths, C., Myers, J., Williams, G., Mikellides, I. G., Hofer, R. R., Polk, J. E., and Jorns, B. A. "Performance Characterization of the Solar Electric Propulsion Technology Demonstration Mission 12.5-kW Hall Thruster," *34th International Electric Propulsion Conference*. Kobe, Japan, 2015.
48. Myers, J., Kamhawi, H., and Yim, J. "HERMeS Thermal Model," *51st Joint Propulsion Conference*. Orlando, FL, 2015.
49. Goebel, D. M., Polk, J. E., Mikellides, I. G., and Lopez Ortega, A. "Lanthanum Hexaboride Hollow Cathode for the Asteroid Retrieval/Redirect Mission," *34th International Electric Propulsion Conference*. Kobe, Japan, 2015.
50. Polk, J. E., Guerrero, P., Goebel, D. M., Mikellides, I. G., and Katz, I. "Thermal Characteristics of Lanthanum Hexaboride Hollow Cathodes," *34th International Electric Propulsion Conference*. Kobe, Japan, 2015.
51. Sekerak, M., Hofer, R. R., Polk, J. E., Jorns, B. A., and Mikellides, I. G. "Wear Testing of a Magnetically Shielded Hall Thruster at 2000 s Specific Impulse," *34th International Electric Propulsion Conference*. Kobe, Japan, 2015.
52. Shastry, R., Huang, W., and Kamhawi, H. "Near-Surface Plasma Characterization of the 12.5-kW NASA TDU1 Hall Thruster," *51st Joint Propulsion Conference*. Orlando, FL, 2015.
53. Huang, W., Kamhawi, H., Myers, J., Yim, J., and Neff, G. "Non-Contact Thermal Characterization of NASA's 12.5-kW Hall Thruster," *51st Joint Propulsion Conference*. Orlando, FL, 2015.
54. Williams, G. J., and Kamhawi, H. "Optical characterization of component wear and near-field plasma of the HERMeS thruster," *62nd JANNAF Propulsion Meeting*. Nashville, TN, 2015.
55. Yim, J. T., and Burt, J. M. "Characterization of vacuum facility background gas through simulation and considerations for electric propulsion ground testing," *51st Joint Propulsion Conference*. Orlando, FL, 2015.

56. Huang, W., and Shastry, R. "Analysis of Wien filter spectra from Hall thruster plumes," *Review of Scientific Instruments* Vol. 86, No. 7, 2015, p. 073502.
doi: 10.1063/1.4923282
57. Huang, W., Kamhawi, H., Myers, J., Yim, J., and Neff, G. "Non-Contact Thermal Characterization of NASA's 12.5-kW Hall Thruster," *To be Presented at the 51st AIAA/SAE/ASEE Joint Propulsion Conference*. Orlando, FL, 2015.
58. Hofer, R. R., and Kamhawi, H. "Development Status of the 12.5 kW HERMeS Hall Thruster Solar Electric Propulsion Technology Demonstration Mission," *52nd AIAA/SAE/ASEE Joint Propulsion Conference*. Salt Lake City, UT, 2016.
59. Huang, W., Kamhawi, H., and Haag, T. W. "Facility Effect Characterization Test of NASA's HERMeS Hall Thruster," *52nd AIAA/SAE/ASEE Joint Propulsion Conference*. Salt Lake City, UT, 2016.
60. Huang, W., Kamhawi, H., and Haag, T. W. "Plasma Oscillation Characterization of NASA's HERMeS Hall Thruster via High Speed Imaging," *52nd AIAA/SAE/ASEE Joint Propulsion Conference*. Salt Lake City, UT, 2016.
61. Kamhawi, H., Haag, T. W., Huang, W., Herman, D. A., Williams, G. J., Peterson, P. Y., Hofer, R. R., and Mikellides, I. "Performance, Stability, and Pressure Effects Characterization Tests of NASA's 12.5-kW Hall Effect Rocket with Magnetic Shielding (HERMeS) Thruster," *52nd AIAA/SAE/ASEE Joint Propulsion Conference*. Salt Lake City, UT, 2016.
62. Hofer, R. R., and Kamhawi, H. "Development Status of a 12.5 kW Hall Thruster for the Asteroid Redirect Robotic Mission," *35th International Electric Propulsion Conference*. ERPS, Atlanta, GA, 2017.
63. Kamhawi, H., Gilland, J. H., Williams, G., Mackey, J., Huang, W., Haag, T. W., and Herman, D. A. "Performance and Stability Characterization of the HERMeS Thruster with M26 Boron Nitride Discharge Channel," *35th International Electric Propulsion Conference*. ERPS, Atlanta, GA, 2017.
64. Diamant, K. D., Liang, R., and Corey, R. L. "The Effect of Background Pressure on SPT-100 Hall Thruster Performance," *50th AIAA/ASME/SAE/ASEE Joint Propulsion Conference*. AIAA, Cleveland, OH, 2014.
65. Kamhawi, H., Huang, W., Haag, T., and Spektor, R. "Investigation of the Effects of Facility Background Pressure on the Performance and Voltage-Current Characteristics of the High Voltage Hall Accelerator," *50th AIAA/ASME/SAE/ASEE Joint Propulsion Conference and Exhibit, AIAA-3707-2014*. Cleveland, OH, USA, 2014.
66. Huang, W., Kamhawi, H., and Haag, T. W. "Facility Effect Characterization Test of NASA's HERMeS Hall Thruster," *52nd AIAA/SAE/ASEE Joint Propulsion Conference,*. Salt Lake City, UT, 2016.
67. Gilland, J. H., Williams, G. J., Burt, J. M., and Yim, J. "Carbon Back Sputter Modeling for Hall Thruster Testing," *52nd AIAA/SAE/ASEE Joint Propulsion Conference*. Salt Lake City, UT, 2016.
68. Topper, J. L., Rubin, B., Farnell, C., and Yalin, A. P. "Quartz Crystal Microbalance Based System for High-Sensitivity Differential Sputter Yield Measurements," *31st International Electric Propulsion Conference*. Ann Arbor, MI, 2009.
69. Mikellides, I. G., Katz, I., Hofer, R. R., and Goebel, D. M. "Magnetic shielding of walls from the unmagnetized ion beam in a Hall thruster," *Applied Physics Letters* Vol. 102, No. 2, 2013.
doi: 10.1063/1.4776192